The Astrophysical Journal Letters, 941:L10 (6pp), 2022 December 10 https://doi.org/10.3847/2041-8213/aca3ae

Neutrinos from the Brightest Gamma-Ray Burst?

Kohta Murase[1,2,3], Mainak Mukhopadhyay[1], Ali Kheirandish[4], Shigeo S. Kimura[5], and Ke Fang[6]
[1] Department of Physics; Department of Astronomy & Astrophysics; Center for Multimessenger Astrophysics, Institute for Gravitation and the Cosmos, The Pennsylvania State University, University Park, PA 16802, USA; murase@psu.edu
[2] School of Natural Sciences, Institute for Advanced Study, Princeton, NJ 08540, USA
[3] Center for Gravitational Physics and Quantum Information, Yukawa Institute for Theoretical Physics, Kyoto University, Kyoto 606-8502, Japan
[4] Department of Physics & Astronomy; Nevada Center for Astrophysics, University of Nevada, Las Vegas, NV 89154, USA
[5] Frontier Research Institute for Interdisciplinary Sciences; Astronomical Institute, Graduate School of Science, Tohoku University, Sendai 980-8578, Japan
[6] Department of Physics, Wisconsin IceCube Particle Astrophysics Center, University of Wisconsin, Madison, WI 53706, USA
Received 2022 October 27; revised 2022 November 13; accepted 2022 November 16; published 2022 December 8

Abstract

We discuss implications that can be obtained by searches for neutrinos from the brightest gamma-ray burst (GRB), GRB 221009A. We derive constraints on GRB model parameters such as the cosmic-ray loading factor and dissipation radius, taking into account both neutrino spectra and effective areas. The results are strong enough to constrain proton acceleration near the photosphere, and we find that the single burst limits are comparable to those from stacking analysis. Quasi-thermal neutrinos from subphotospheres and ultra-high-energy neutrinos from external shocks are not yet constrained. We show that GeV–TeV neutrinos originating from neutron collisions are detectable, and urge dedicated analysis on these neutrinos with DeepCore and IceCube as well as ORCA and KM3NeT.

Unified Astronomy Thesaurus concepts: Neutrino astronomy (1100); High energy astrophysics (739); Gamma-ray bursts (629); Cosmic rays (329)

1. Introduction

Gamma-ray bursts (GRBs) are the most powerful explosive phenomena in the universe, which have been extensively discussed as ultra-high-energy (UHE) cosmic-ray (CR) accelerators (Vietri 1995; Waxman 1995). Accompanied high-energy neutrinos have been searched for, but no detection has been reported so far (Abbasi et al. 2012; Aartsen et al. 2017a; Albert et al. 2020). Canonical high-luminosity GRBs cannot make a major contribution to the all-sky neutrino flux measured in IceCube, and optimistic cases have been ruled out. The hypothesis that UHE CRs come from GRBs has not yet been excluded, and various possibilities of high-energy CR and neutrino production in GRBs have been investigated (see reviews from Mészáros 2015; Kimura 2022, and references therein).

On 2022 October 9, an extraordinarily bright burst, GRB 221009A, was reported. This burst was reported by Swift-BAT as an unknown-type transient (Dichiara et al. 2022), and it had triggered Fermi-GBM about 1 hr before the BAT trigger time (Veres et al. 2022). The burst showed an initial pulse of $\sim$10 s, followed by the main burst beginning at $\sim$180 s after the GBM trigger time. The preliminary estimate of the gamma-ray energy fluence reported by Konus-Wind is $\sim 5\times 10^{-2}\,\mathrm{erg\,cm^{-2}}$ (Frederiks et al. 2022). Afterglow emission has been observed at different wavelengths, and optical follow-up observations revealed that the redshift of this GRB is $z=0.15$ (de Ugarte Postigo et al. 2022), which suggests that the isotropic-equivalent gamma-ray energy is $\mathcal{E}_\gamma^{\rm iso}\sim 3\times 10^{54}$ erg. The detection of high-energy gamma rays at $\sim$200–600 s after the GBM trigger time was reported by Fermi-LAT. The highest-energy photon of 99 GeV was detected by LAT at 240 s after the trigger (Pillera et al. 2022). The Large High Altitude Air Shower Observatory observed more than 5000 very-high-energy photons in the TeV range, and even $\gtrsim$10 TeV photons were detected (Huang et al. 2022).

In this work, we demonstrate how observations of neutrinos from the brightest GRB can be used for learning about models of GRB neutrino emission. We focus on neutrinos emitted during the prompt phase, and consider not only nonthermal neutrinos accompanied by CR acceleration but also quasi-thermal neutrinos produced by inelastic collisions with neutrons. We use $Q_x=Q/10^x$ in CGS units and assume cosmological parameters with $\Omega_m=0.3$, $\Omega_\Lambda=0.7$ and $h=0.7$.

2. Nonthermal Emission

2.1. Gamma-Ray Constraints

The detection of high-energy gamma rays can be used for placing a lower limit on the bulk Lorentz factor Γ (e.g., Lithwick & Sari 2001) and/or the dissipation radius $r_{\rm diss}$ (e.g., Gupta & Zhang 2008; Murase & Ioka 2008; Zhang & Pe'er 2009). The detection of a $\sim$100 GeV photon at $\sim$240 s after the trigger (Pillera et al. 2022) suggests that the emission region has to be transparent to $\gamma\gamma\to e^+e^-$. The two-photon annihilation optical depth for a gamma ray with energy ε_γ is

$$\tau_{\gamma\gamma}\simeq 150\frac{\eta_{\gamma\gamma,-1}L_{\gamma,52.5}}{r_{\rm diss,14}\Gamma_{2.5}^2\varepsilon^b_{\rm MeV}}\begin{cases}(\varepsilon_\gamma/\varepsilon_\gamma^b)^{\beta-1} & (\varepsilon_\gamma<\varepsilon_\gamma^b)\\ (\varepsilon_\gamma/\varepsilon_\gamma^b)^{\alpha-1} & (\varepsilon_\gamma^b<\varepsilon_\gamma)\end{cases}, \quad (1)$$

where $\eta_{\gamma\gamma}\sim 0.1$ is a spectrum-dependent coefficient (Svensson 1987), L_γ is the isotropic-equivalent gamma-ray luminosity during the main brightest episode, where we take $10^{52.5}\,\mathrm{erg\,s^{-1}}$ in the Konus-Wind band (so that the band correction is included), $\varepsilon^b\equiv 1$ MeV $\varepsilon^b_{\rm MeV}$ is the photon break energy in the GRB frame, and α and β are low- and high-energy photon indices, respectively. The typical energy of high-energy gamma rays

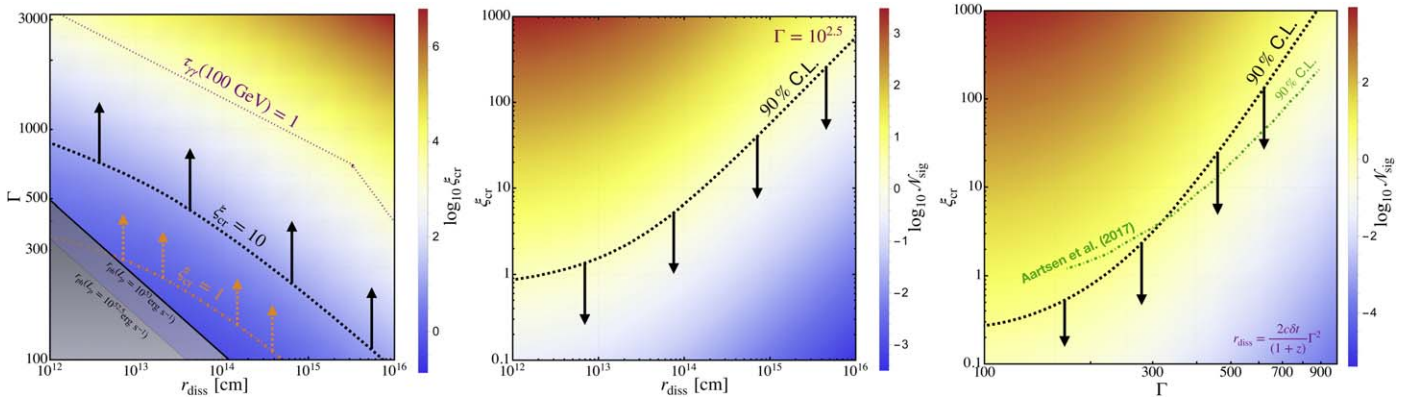

Figure 1. (Left) Constraints on Γ as a function of $r_{\rm diss}$ for different values of the CR loading factor $\xi_{\rm cr}$. The region below $r_{\rm ph}$ is not considered for nonthermal neutrino production. (Middle) Constraints on $\xi_{\rm cr}$ as a function of $r_{\rm diss}$ for a given Lorentz factor of $\Gamma = 10^{2.5}$. (Right) Constraints on $\xi_{\rm cr}$ as a function of Γ in the internal shock model, where the IceCube stacking limit at 90% C.L. (Aartsen et al. 2017a) is also shown. Note that color scale represents the number of signal events $\mathcal{N}_{\rm sig}$.

interacting with target photons at a break energy is $E_\gamma^b = \varepsilon_\gamma^b/(1+z) \approx \Gamma^2 m_e^2 c^4/\varepsilon^b/(1+z) \simeq 23\ \mathrm{GeV}\ \Gamma_{2.5}^2(\varepsilon_{\rm MeV}^b)^{-1}$ for GRB 221009A.

Requiring $\tau_{\gamma\gamma}(E_\gamma = 100\,\mathrm{GeV}) < 1$, with $\varepsilon^b \sim 1\,\mathrm{MeV}$, $\alpha \sim 1.0$, and $\beta \sim 2.6$ (Frederiks et al. 2022), the dissipation radius can be constrained as

$$r_{\rm diss} \gtrsim 1.5 \times 10^{16}\ \mathrm{cm}\ L_{\gamma,52.5}\Gamma_{2.5}^{-2}\begin{cases} 1 & (\Gamma \lesssim 700) \\ (5\Gamma_{2.5}^{-2})^{1.6} & (\Gamma \gtrsim 700) \end{cases}. \quad (2)$$

We also obtain $\Gamma \gtrsim 770\,(L_{\gamma,52.5}\delta t_{-2}^{-1})^{5/36}$ with $r_{\rm diss} \approx 2\Gamma^2 c\delta t/(1+z)$ that is expected in the internal shock scenario (where δt is the variability timescale), although this constraint can be relaxed in multizone models (Aoi et al. 2010). High-energy gamma rays with $\varepsilon_\gamma \gg 1\,\mathrm{GeV}$ are unlikely to be produced near the photosphere, as has been argued for some of the past bright GRBs (e.g., Zhang & Pe'er 2009).

2.2. Neutrino Constraints

If the high-energy CRs are accelerated during the prompt phase, they should interact with GRB photons via the photomeson production process (Waxman & Bahcall 1997), leading to a flux of high-energy neutrinos via decay processes like $\pi^+ \to \mu^+\nu_\mu \to \nu_\mu\bar{\nu}_\mu\nu_e e^+$. The effective $p\gamma$ optical depth is (e.g., Waxman & Bahcall 1997; Murase et al. 2006)

$$f_{p\gamma} \simeq 0.15\frac{\eta_{p\gamma}L_{\gamma,52.5}}{r_{\rm diss,14}\Gamma_{2.5}^2\varepsilon_{\rm MeV}^b}\begin{cases}(\varepsilon_p/\varepsilon_p^b)^{\beta-1} & (\varepsilon_p < \varepsilon_p^b) \\ (\varepsilon_p/\varepsilon_p^b)^{\alpha-1} & (\varepsilon_p^b < \varepsilon_p)\end{cases}, \quad (3)$$

where $\varepsilon_p^b \approx 0.5\bar{\varepsilon}_\Delta m_p c^2\Gamma^2/\varepsilon^b$ is the proton break energy in the GRB frame, and $\bar{\varepsilon}_\Delta \sim 0.3$ GeV. Here $\eta_{p\gamma}$ is a correction factor that is $\sim(2-3)$ for $\alpha \sim 1$ due to the effects of multipion production and high inelasticity (Murase & Nagataki 2006). The resulting typical neutrino energy is $E_\nu^b \approx 0.05\varepsilon_p^b/(1+z) \sim 0.6\ \mathrm{PeV}\ \Gamma_{2.5}^2(\varepsilon_{\rm MeV}^b)^{-1}$.

By introducing the CR loading factor $\xi_{\rm cr} \equiv \mathcal{E}_{\rm cr}^{\rm iso}/\mathcal{E}_\gamma^{\rm iso}$ (Murase & Nagataki 2006), the neutrino fluence is estimated to be

$$E_\nu^2\phi_{\nu_\mu} \approx \frac{1}{8}\frac{(1+z)}{4\pi d_L^2}\min[1, f_{p\gamma}]\xi_{\rm cr}\frac{\mathcal{E}_\gamma^{\rm iso}}{\mathcal{R}_{\rm cr}} \sim 4\times10^{-3}\ \mathrm{erg\ cm^{-2}}\ \min[1, f_{p\gamma}]\xi_{\rm cr,1}\mathcal{E}_{\gamma,54.5}^{\rm iso}\mathcal{R}_{\rm cr,1.2}^{-1}, \quad (4)$$

where $1/8$ comes from the fact that the $\pi^\pm/\pi^0$ ratio is ~ 1 in $p\gamma$ interactions due to the contribution from direct production and each flavor of neutrinos after the mixing carries $\sim 1/4$ of the pion energy in the decay chain. Also, $\mathcal{R}_{\rm cr}$ is a spectrum-dependent factor that converts the bolometric CR energy to the differential CR energy, which is $\mathcal{R}_{\rm cr} \sim 15$–$20$ for a CR spectral index of $s_{\rm cr} = 2.0$ depending on the CR maximum energy.

Nondetection of neutrinos from GRB 221009A was reported by IceCube Collaboration (2022), which gives $E_\nu^2\phi_{\nu_\mu} \leqslant 3.9\times10^{-2}\,\mathrm{GeV\,cm^{-2}}$ at 90% C.L. for an E_ν^{-2} spectrum. This naively infers

$$\min[\xi_{\rm cr,-1}, f_{p\gamma,-2}\,\xi_{\rm cr,1}] \lesssim 2. \quad (5)$$

However, this constraint is optimistic and it should not be used in general cases. Since GRB neutrino spectra are not described by a single power law, it is significantly relaxed when E_ν^b is higher than 10–100 TeV, the regime in which IceCube is the most sensitive (Abbasi et al. 2021a).

Because the dissipation radius of prompt emission is not well known and is under debate, it is often more useful to treat $r_{\rm diss}$ as an uncertain parameter (Murase et al. 2008; Zhang & Kumar 2013). In Figure 1, the left and middle, we present constraints in the $r_{\rm diss} - \Gamma$ plane (see also Gao et al. 2013, for GRB 130427A) and $r_{\rm diss} - \xi_{\rm cr}$ plane, respectively. The neutrino spectra are calculated using the prescription in He et al. (2012) and Kimura et al. (2017), assuming $\xi_B = 1$ for magnetic fields (Murase & Nagataki 2006). We adopt $\varepsilon^b = 1.2\,\mathrm{MeV}$, $\alpha = 1.1$, and $\beta = 2.6$ (Frederiks et al. 2022), which is sufficient for the purpose of this work to demonstrate the constraints and to encourage further searches with detailed information on time-dependent spectra. We use the point-source effective area[7]

[7] In general the gamma-ray follow-up effective area (Aartsen et al. 2017b) should be used for real time follow-ups. But the publicly available data do not have a sufficiently fine binning in the zenith angle.

(Abbasi et al. 2021b) at decl. $\delta \approx 19^{\circ}.8$. The convolution of the neutrino flux and the effective area over a relevant energy range ($200\,\mathrm{GeV} \leqslant E_\nu \leqslant 10^9\,\mathrm{GeV}$) gives the number of signal events, $\mathcal{N}_{\rm sig}$. Our limit for an E_ν^{-2} spectrum also agrees with the IceCube limit (IceCube Collaboration 2022). The results on $\mathcal{N}_{\rm sig}$ are not strongly affected by ξ_B. This is because the signal mainly comes from neutrinos around E_ν^b, whereas ξ_B is important for the neutrino flux suppression that occurs at much higher energies at ∼10–1000 PeV (Murase & Nagataki 2006).

Remarkably, we obtain strong constraints on particle acceleration near the photosphere at $r_{\rm ph} \simeq 3.8 \times 10^{12}\,\mathrm{cm}\,\zeta_e L_{p,53}\Gamma_{2.5}^{-3}$ in the limit that the coasting occurs under $r_{\rm ph}$. Here L_p is the proton luminosity and ζ_e is the number ratio of electrons and positrons to protons. From Figure 1, the left and middle, we obtain $\xi_{\rm cr} \lesssim 1$ for $\Gamma \lesssim 300$, which excludes the benchmark case of the baryonic photospheric scenario ($\xi_{\rm cr} = 1$ and $\zeta_e = 1$), although the limits can be relaxed with larger values of Γ. Note that these constraints on the baryonic photospheric scenario are largely insensitive to uncertainty in L_γ because of $f_{p\gamma} \sim 20(L_{\gamma,52.5}/L_{p,53})(\Gamma_{2.5}/\varepsilon_{\rm MeV}^b)\tau_T \gg 1$ near the photosphere (Murase 2008), where τ_T is the Thomson optical depth. Our results are conservative in the sense that we do not include *pp* collisions that are relevant in the TeV range (Murase 2008; Wang & Dai 2009).

On the other hand, IceCube's nondetection is consistent with outer-zone (i.e., large $r_{\rm diss}$) models. For example, we obtain $r_{\rm diss} \gtrsim (2\text{–}20) \times 10^{14}$ cm for $\Gamma \sim 300$ and $\xi_{\rm cr} \sim 10\text{–}100$. Such parameter space is favored by the scenario where UHE CRs are nuclei rather than protons (see Figure 8 of Murase et al. 2008) and some of the magnetic reconnection models (e.g., Zhang & Kumar 2013; Pitik et al. 2021). This also rules out the neutron escape scenario for UHE CRs (Ahlers et al. 2011). We also note that low efficiencies of the photomeson production process are also consistent with the detection of a ∼100 GeV photon. From Equations (2) and (3) we obtain

$$f_{p\gamma} \lesssim 3 \times 10^{-3}\,\eta_{p\gamma,0.5}\begin{cases}1 & (\Gamma \lesssim 700)\\ (\Gamma_{2.5}^2/5)^{1.6} & (\Gamma \gtrsim 700)\end{cases}. \quad (6)$$

This limit does not depend on L_γ and $r_{\rm diss}$, and it is applicable to all proton energies given $\alpha \sim 1$. Although Equation (6) is robust as long as neutrinos and gamma rays are coproduced, it is worthwhile to note that their emission regions may be different. For example, in the photospheric scenario, sub-TeV gamma rays are unlikely to escape and hence should come from large dissipation radii, e.g., at the external reverse shock (Zhang et al. 2022).

Prompt GRB neutrinos have been best studied in the context of the internal shock scenario, and the UHE CR hypothesis requires $\xi_{\rm cr} \sim 10\text{–}100$ (Murase et al. 2008; Biehl et al. 2018). The constraints with the assumption of $r_{\rm diss} \approx 2\Gamma^2 c\delta t/(1+z)$ are presented in Figure 1, on the right. Here, for the purpose of the comparison with the IceCube result (Aartsen et al. 2017a), we use $\delta t = 0.01$ s, although the chosen value is subject to both observational and model uncertainties (e.g., Murase & Nagataki 2006; Murase et al. 2008; Zhang & Kumar 2013).

We find $\xi_{\rm cr} \lesssim 3$ for $\Gamma = 300$. This implies that for a benchmark Lorentz factor of $\Gamma = 300$ that is often used in the literature (e.g., Aartsen et al. 2017a), the case motivated by the UHE CR hypothesis may be excluded, where the constraint given in Equation (2) should be alleviated if neutrinos and the highest-energy gamma rays come from different regions (e.g., Bustamante et al. 2015; Zhang et al. 2022). Alternatively, GRB internal shocks are still viable for UHE CR acceleration if the Lorentz factor is high enough to lead to large $r_{\rm diss} \gtrsim (2\text{–}20) \times 10^{14}$ cm, as used in Murase et al. (2008). Interestingly, our new limit shown in Figure 1 is comparable to the IceCube stacking limit (Aartsen et al. 2017a). Our results are useful because the latter is subject to systematic uncertainties coming from the aggregation of many bursts. One single burst provides complementary constraints, and supports that canonical high-luminosity GRBs contribute less than ∼1% of the all-sky neutrino flux.

3. Quasi-thermal Emission

Subphotospheric neutrino production at $\tau_{\rm T} \gtrsim 1$ is efficient if CRs exist. However, CR acceleration at radiation-mediated shocks is inefficient, and the detection of nonthermal neutrinos from deep subphotospheres is unlikely for canonical high-luminosity GRBs (Murase & Ioka 2013; Bhattacharya et al. 2022). However, high-energy neutrinos can still be produced without relying on CR acceleration. Neutrons can provide neutrinos through inelastic collisions between bulk flows or neutron diffusion (Mészáros & Rees 2000), without involving collisionless shocks or magnetic reconnections. Such "quasi-thermal" neutrinos are naturally produced during neutron decoupling (Bahcall & Meszaros 2000) and/or by internal collisions between neutron-loaded outflows (Bartos et al. 2013; Murase et al. 2013; Zegarelli et al. 2022).

3.1. Neutrinos from Neutron Decoupling

Recent studies have shown that a GRB jet is collimated during its propagation inside a star (e.g., Bromberg et al. 2011; Mizuta & Ioka 2013; Hamidani & Ioka 2020; Gottlieb et al. 2022). The jet material becomes hot and the postcollimation density is so high that $\tau_{\rm T} \gg \tau_{np} \gg 1$, in which protons and neutrons are coupled. After the breakout, the hot jet material may expand with $\Gamma(r) \approx \Gamma_*(r/R_*)$ like a fireball, where $\Gamma_* \approx 1/\theta_j = 10\,\theta_{j,-1}^{-1}$ is the Lorentz factor at the breakout. By equating the *np* collision time $t_{np} \approx 1/(n'_p\,\sigma_{np}c)$ (where $\sigma_{np} \approx 3 \times 10^{-26}\,\mathrm{cm}^2$ is the approximate *np* cross section, $n'_p \approx L_p/(4\pi r^2 \Gamma\Gamma_{\rm max} m_p c^3)$ is the proton density, and $\Gamma_{\rm max}$ is the maximum Lorentz factor) and the expansion time $t_{\rm dyn} \approx r/(\Gamma c)$, the decoupling radius is estimated to be $r_{\rm dec} \approx 8.7 \times 10^{11}\,\mathrm{cm}\,L_{p,53}^{1/3}R_{*,11}^{2/3}\Gamma_{*,1}^{-2/3}\Gamma_{\rm max,2.9}^{-1/3}$, at which the Lorentz factor becomes

$$\Gamma_{n,\rm dec} \approx 65\;L_{p,53}^{1/3}R_{*,11}^{-1/3}\Gamma_{*,1}^{1/3}\Gamma_{\rm max,2.9}^{-1/3}, \quad (7)$$

where a numerical factor of 3/4 is taken into account. Note that the decoupling during the acceleration occurs if $\Gamma_{\rm max}$ is larger than the critical value;

$$\Gamma_{np} \approx \left(\frac{\sigma_{np}L_p\Gamma_*}{4\pi m_p c^3 R_*}\right)^{1/4}. \quad (8)$$

Radiative acceleration is fast and the flow is accelerated relativistically, in which inelastic *np* collisions occur during the neutron decoupling (Bahcall & Meszaros 2000). The *np* optical depth is around unity at the decoupling radius by definition, and the energy of quasi-thermal neutrinos is (Bahcall & Meszaros 2000)

$$E_\nu^{\rm qt} \approx 0.1\Gamma_{n,\rm dec} m_p c^2/(1+z), \quad (9)$$

which predicts ∼1–10 GeV neutrinos.

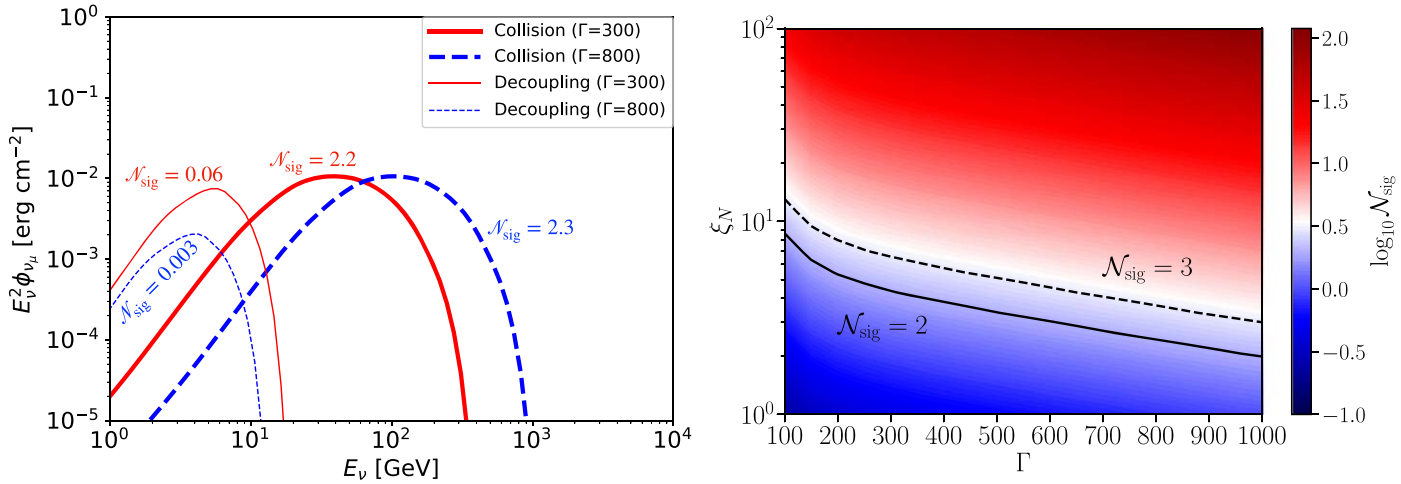

Figure 2. Left) Energy fluences of quasi-thermal ν_μ from GRB 221009A for both collision and decoupling scenarios, where $\xi_N = 5$ and $\mathcal{E}_\gamma^{\rm iso} = 10^{54.5}$ erg are used. (Right) Expected number of signal events, $\mathcal{N}_{\rm sig}$, in DeepCore+IceCube as a function of ξ_N and Γ. The solid and dashed lines show the parameter sets that lead to doublet and triplet events, respectively.

The neutrino energy fluence is estimated to be

$$E_\nu^2\phi_{\nu_\mu} \approx \frac{1}{12}\frac{(1+z)}{4\pi d_L^2}\zeta_n\left(\frac{\Gamma_{n,\rm dec}}{\Gamma}\right)\xi_N\mathcal{E}_\gamma^{\rm iso} \sim 0.01\ {\rm erg\ cm^{-2}}\ \zeta_n(\Gamma_{n,\rm dec}/0.2\Gamma)\xi_{N,1}\mathcal{E}_{\gamma,54.5}^{\rm iso}, \quad (10)$$

where a nucleon inelasticity of $\approx$0.5 in *np* collisions is taken into account, and the other $1/6$ comes from the fact that $2/3$ of pions produced by *np* collisions are charged pions and $3/4$ of their decay products are equally shared by each flavor of neutrinos after the neutrino mixing.[8] Also, ζ_n is the number ratio of neutrons to protons, $\xi_N\mathcal{E}_\gamma^{\rm iso}$ is the kinetic energy of the proton outflow with $\Gamma \gtrsim \Gamma_{n,\rm dec}$ and ξ_N is the nucleon loading factor.

In Figure 2, to the left, we show neutrino fluences in the neutron "decoupling" model with $\zeta_n = 1$. We set $\Gamma_{n,\rm dec}$ from Equation (7) assuming $\Gamma = \Gamma_{\rm max}$. The spectra of neutrinos from *np* collisions are calculated with `Geant4` following Murase et al. (2013).

3.2. Neutrinos from Colliding Neutron-loaded Flows

If the neutron decoupling occurs before $\Gamma \approx \Gamma_{\rm max}$ is achieved, the neutron flow will be caught up by the proton flow, leading to *pn* collisions (Beloborodov 2010; Mészáros & Rees 2011). Alternatively, if the coasting occurs earlier than the decoupling, the dissipation of neutrons via internal collisions between the compound flows may happen. Such collisions are expected around $r_{\rm dec} \ll r_{\rm ph}$, where the *pn* optical depth is $\tau_{pn} \approx 1\,(\Gamma/\Gamma_{n,\rm dec})(\zeta_n/\zeta_e)\tau_T$. The typical energy of neutrinos is given by Murase et al. (2013) as

$$E_\nu^{\rm qt} \approx 0.1\Gamma\Gamma'_{\rm rel}m_pc^2/(1+z), \quad (11)$$

where $\Gamma'_{\rm rel} \sim 2$ is the relative Lorentz factor of the interacting flow and $\sim$30–300 GeV neutrinos are expected for $\Gamma \sim 10^2$–10^3.

[8] This is a good approximation especially for successful jets but neutrinos produced deep inside a star are subject to neutrino oscillation due to effects of matter and neutrino self-interaction (Carpio & Murase 2020; Abbar et al. 2022).

The neutrino energy fluence is

$$E_\nu^2\phi_{\nu_\mu} \approx \frac{1}{12}\frac{(1+z)}{4\pi d_L^2}\tau_{pn}\xi_N\mathcal{E}_\gamma^{\rm iso} \sim 0.03\ {\rm erg\ cm^{-2}}\ \tau_{pn}\xi_{N,1}\mathcal{E}_{\gamma,54.5}^{\rm iso}, \quad (12)$$

where the normalization is set by $\xi_N\mathcal{E}_\gamma^{\rm iso}$ as the kinetic energy of the interacting flow. It has been suggested that dissipation induced by internal collisions between neutron-loaded flows may be relevant for subphotospheric dissipation (Beloborodov 2010; Mészáros & Rees 2011), in which $E_\nu^2\phi_\nu \sim E_\gamma^2\phi_\gamma$ and $\xi_N \sim$ 3–30 can be considered as fiducial values.

In Figure 2, on the left, we show neutrino fluences in the "collision" model for $\Gamma = 300$ and $\Gamma = 800$, where $\tau_{pn} = 1$ is assumed.

3.3. Implications

We calculate the number of signal events using the latest all-flavor effective areas for GRECO selection (Abbasi et al. 2022) and through-going muon neutrinos (Abbasi et al. 2021b) in IceCube. The values of $\mathcal{N}_{\rm sig}$ for different models are shown in Figure 2, on the left. Although the decoupling model is difficult to test with IceCube and other detectors such as KM3Net and Baikal-GVD, we find that the collision model is promising. A few events of $\sim$100 GeV neutrinos can be detected for $\xi_N \sim 10$ especially if the Lorentz factor is sufficiently large (e.g., $\Gamma \sim 800$). These results are encouraging and we urge dedicated searches for GeV–TeV neutrinos for GRB 221009A with the existing IceCube data.

In Figure 2 right, we also show the sensitivity to ξ_N as a function of Γ for double and triplet detections of signal neutrinos from GRB 221009A. Although the expected signal can dominate if angular uncertainty is not far from the kinematic angle (Murase et al. 2013), the actual detectability depends on the atmospheric background rate, so dedicated analyses at sub-TeV energies are necessary. A search time window (ΔT) will also need to be carefully considered. The burst duration may vary depending on energy bands (e.g., Zhang et al. 2014), and the engine duration is uncertain. Neutrino emission may be dominated by the main episode that

lasts for $\Delta T \sim 100$ s, and luminosity-weighted searches could also be helpful more generally.

Note that in both the decoupling and collision models, neutrinos and gamma rays are mainly produced deep inside the photosphere, from which gamma rays with $\varepsilon_\gamma \gtrsim \Gamma m_e c^2$ cannot escape (e.g., Murase & Ioka 2008). Residual neutrons would eventually decay after $\sim 880/\Gamma_{n,\rm dec}$ s in the observer frame, but the resulting electron antineutrino energy is $\sim 0.48\,\Gamma_{n,\rm dec}$ MeV, which is difficult to detect with IceCube-like detectors. Electrons may lose their energies via synchrotron and inverse-Compton emission but their signatures may easily be overwhelmed by other components.

4. Summary and Discussion

We considered how observations of neutrinos from the brightest GRB can be used for constraining GRB model parameters, including the CR baryon loading factor that is a critical parameter for the production of high-energy neutrinos and UHE CRs. We showed that the IceCube nondetection of TeV–PeV neutrinos from GRB 221009A leads to intriguing constraints on the parameter space of $r_{\rm diss}$, Γ, and $\xi_{\rm cr}$, which are comparable to those from the stacking analysis that is subject to systematics from many GRBs with different properties. We found that CR acceleration near the photosphere is likely to be subdominant and obtained $\xi_{\rm cr} \lesssim 1$ for $\Gamma \lesssim 300$. We also pointed out that the nondetection of high-energy nonthermal neutrinos is not surprising in light of the gamma-ray constraint. This is consistent with outer-zone models (e.g., Murase et al. 2008; Zhang & Kumar 2013). However, neutrinos and gamma rays may come from different dissipation regions, and further investigation with multizone models (Bustamante et al. 2017; Rudolph et al. 2020) might be relevant.

Quasi-thermal neutrinos, which are naturally expected if neutrons are loaded into GRB outflows, are not yet constrained. We found that in the collision model the detection of GeV–TeV neutrinos is possible with IceCube's low- and high-energy channels, or reasonable constraints on ξ_N can be obtained. Even higher-energy neutrinos may be produced via the neutron-proton-converter acceleration mechanism (Kashiyama et al. 2013), and we encourage dedicated searches by considering appropriate time windows focusing on the bright episodes of prompt emission.

Finally, we note that UHE CRs could be accelerated by external shocks during the early afterglow phase (Waxman & Bahcall 2000; Murase 2007; Razzaque 2013), in which PeV–EeV neutrinos are expected and the predicted fluxes have not been reached by the current IceCube. Future UHE neutrino detectors (Ackermann et al. 2022) such as IceCube-Gen2, Trinity, and GRAND will be required to test those afterglow models.

We thank Francis Halzen and Kazumi Kashiyama for discussions. The work of K.M. and M.M. is supported by the NSF grant No. AST-2108466. K.M. also acknowledges support from the NSF grant Nos. AST-1908689, AST-2108467, and KAKENHI Nos. 20H01901 and 20H05852. M.M. also acknowledges support from the Institute for Gravitation and the Cosmos (IGC) Postdoctoral Fellowship. A.K. acknowledges support from Nevada Center for Astrophysics. S.S.K. acknowledges support by the Tohoku Initiative for Fostering Global Researchers for Interdisciplinary Sciences (TI-FRIS) of MEXTs Strategic Professional Development Program for Young Researchers. The work of K.F. is supported by the Office of the Vice Chancellor for Research and Graduate Education at the University of Wisconsin-Madison with funding from the Wisconsin Alumni Research Foundation. K.F. acknowledges support from NASA (NNH19ZDA001N-Fermi, NNH20ZDA001N-Fermi) and National Science Foundation (PHY-2110821).

While we were finalizing the manuscript, the related work (Ai & Gao 2022) came out. The approaches are different, and we impose constraints on GRB parameters based on projecting expected events with model spectra, instead of the reported single power-law upper limit. Our study also includes calculations of nonthermal as well as quasi-thermal neutrinos.

ORCID iDs

Kohta Murase https://orcid.org/0000-0002-5358-5642
Mainak Mukhopadhyay https://orcid.org/0000-0002-2109-5315
Ali Kheirandish https://orcid.org/0000-0001-7074-0539
Shigeo S. Kimura https://orcid.org/0000-0003-2579-7266
Ke Fang https://orcid.org/0000-0002-5387-8138

References

Aartsen, M. G., Ackermann, M., Adams, J., et al. 2017a, ApJ, 843, 112
Aartsen, M. G., Ackermann, M., Adams, J., et al. 2017b, APh, 92, 30
Abbar, S., Carpio, J. A., & Murase, K. 2022, arXiv:2205.10384
Abbasi, R., Abdou, Y., Abu-Zayyad, T., et al. 2012, Natur, 484, 351
Abbasi, R., Ackermann, M., Adams, J., et al. 2021a, ApJ, 910, 4
Abbasi, R., Ackermann, M., Adams, J., et al. 2021b, arXiv:2101.09836
Abbasi, R., Ackermann, M., Adams, J., et al. 2022, JCAP, 01, 027
Ackermann, M., Bustamante, M., Lu, L., et al. 2022, JHEAp, 36, 55
Ahlers, M., Gonzalez-Garcia, M. C., & Halzen, F. 2011, APh, 35, 87
Ai, S., & Gao, H. 2022, arXiv:2210.14116
Albert, A., André, M., Anghinolfi, M., et al. 2020, MNRAS, 500, 5614
Aoi, J., Murase, K., Takahashi, K., Ioka, K., & Nagataki, S. 2010, ApJ, 722, 440
Bahcall, J. N., & Mészáros, P. 2000, PhRvL, 85, 1362
Bartos, I., Beloborodov, A. M., Hurley, K., & Marka, S. 2013, PhRvL, 110, 241101
Beloborodov, A. M. 2010, MNRAS, 407, 1033
Bhattacharya, M., Carpio, J. A., Murase, K., & Horiuchi, S. 2022, arXiv:2210.08029
Biehl, D., Heinze, J., & Winter, W. 2018, MNRAS, 476, 1191
Bromberg, O., Nakar, E., Piran, T., & Sari, R. 2011, ApJ, 740, 100
Bustamante, M., Baerwald, P., Murase, K., & Winter, W. 2015, NatCo, 6, 6783
Bustamante, M., Heinze, J., Murase, K., & Winter, W. 2017, ApJ, 837, 33
Carpio, J. A., & Murase, K. 2020, PhRvD, 101, 123002
de Ugarte Postigo, A., Izzo, L., Pugliese, G., et al. 2022, GCN, 32648, 1
Dichiara, S., Gropp, J., Kennea, J., et al. 2022, GCN, 32632, 1
Frederiks, D., Lysenko, A., Ridnaia, A., et al. 2022, GCN, 32668, 1
Gao, S., Kashiyama, K., & Mészáros, P. 2013, ApJL, 772, L4
Gottlieb, O., Liska, M., Tchekhovskoy, A., et al. 2022, ApJL, 933, L9
Gupta, N., & Zhang, B. 2008, MNRAS, 384, L11
Hamidani, H., & Ioka, K. 2020, MNRAS, 500, 627
He, H.-N., Liu, R.-Y., Wang, X.-Y., et al. 2012, ApJ, 752, 29
Huang, Y., Hu, S., Chen, S., et al. 2022, GCN, 32677, 1
IceCube Collaboration 2022, GCN, 32665, 1
Kashiyama, K., Murase, K., & Meszaros, P. 2013, PhRvL, 111, 131103
Kimura, S. S. 2022, arXiv:2202.06480
Kimura, S. S., Murase, K., Mészáros, P., & Kiuchi, K. 2017, ApJ, 848, L4
Lithwick, Y., & Sari, R. 2001, ApJ, 555, 540
Mészáros, P. 2015, arXiv:1511.01396
Mészáros, P., & Rees, M. J. 2000, ApJL, 541, L5
Mészáros, P., & Rees, M. J. 2011, ApJL, 733, L40
Mizuta, A., & Ioka, K. 2013, ApJ, 777, 162
Murase, K. 2007, PhRvD, 76, 123001
Murase, K. 2008, PhRvD, 78, 101302 R
Murase, K., & Ioka, K. 2008, ApJ, 676, 1123
Murase, K., & Ioka, K. 2013, PhRvL, 111, 121102
Murase, K., Ioka, K., Nagataki, S., & Nakamura, T. 2006, ApJ, 651, L5

Murase, K., Ioka, K., Nagataki, S., & Nakamura, T. 2008, PhRvD, 78, 023005
Murase, K., Kashiyama, K., & Meszaros, P. 2013, PhRvL, 111, 131102
Murase, K., & Nagataki, S. 2006, PhRvD, 73, 063002
Pillera, R., Bissaldi, E., Omodei, N., La Mura, G., & Longo, F. 2022, ATel, 15656, 1
Pitik, T., Tamborra, I., & Petropoulou, M. 2021, JCAP, 05, 034
Razzaque, S. 2013, PhRvD, 88, 103003
Rudolph, A., Heinze, J., Fedynitch, A., & Winter, W. 2020, ApJ, 893, 72
Svensson, R. 1987, MNRAS, 227, 403
Veres, P., Burns, E., Bissaldi, E., et al. 2022, GCN, 32636, 1
Vietri, M. 1995, ApJ, 453, 883
Wang, X.-Y., & Dai, Z.-G. 2009, ApJ, 691, L67
Waxman, E. 1995, PhRvL, 75, 386
Waxman, E., & Bahcall, J. 1997, PhRvL, 78, 2292
Waxman, E., & Bahcall, J. N. 2000, ApJ, 541, 707
Zegarelli, A., Celli, S., Capone, A., et al. 2022, PhRvD, 105, 083023
Zhang, B., & Kumar, P. 2013, PhRvL, 110, 121101
Zhang, B., & Pe'er, A. 2009, ApJL, 700, L65
Zhang, B.-B., Zhang, B., Murase, K., Connaughton, V., & Briggs, M. S. 2014, ApJ, 787, 66
Zhang, B. T., Murase, K., Ioka, K., et al. 2022, arXiv:2211.05754